Turkish Journal of Electrical Engineering & Computer Sciences

http://journals.tubitak.gov.tr/elektrik/

Research Article

Turk J Elec Eng & Comp Sci
(2021) 29: 1106 – 1123

doi:10.3906/elk-2006-91

Analytical modeling and study on noise characteristics of rotor eccentric SPMSM with unequal magnetic poles structure

Pengpeng XIA, Shenbo YU*, Rutong DOU, Fengchen ZHAI
School of Mechanical Engineering, Shenyang University of Technology, Shenyang, China

Received: 17.06.2020 • **Accepted/Published Online:** 11.09.2020 • **Final Version:** 30.03.2021

Abstract: The establishment of the analytical model of the rotor eccentric surface-mounted permanent magnet synchronous motor (SPMSM) with unequal magnetic poles structure will be beneficial to calculating the magnetic field and studying noise characteristics quickly. Based on the equivalent surface current (ESC) method and equivalent boundary method, the analytical model of the rotor eccentric SPMSM with unequal magnetic poles structure is proposed. During the modeling process, the magnetic field produced by a permanent magnet (PM) is obtained using the ESC method, and the effect on the air gap magnetic field, which arised from stator, is replaced with the concentric current sheet (CCS) magnetic field. And, the analytical results of the magnetic field are confirmed by FEM. According to the analytical model of the SPMSM, the effect on the noise characteristics, which resulted from rotor eccentricity, is researched. Moreover, the experiments of noise comparison are done. The results validate the validity of noise characteristic research. Then, the analytical model of the SPMSM is further verified.

Key words: Analytical method, rotor eccentricity, surface-mounted permanent magnet synchronous motor (SPMSM), unequal magnetic poles structure, noise characteristics

1. Introduction

Because of the characteristics of high power density and efficiency, the SPMSM has been used in industrial manufacture, home automation, etc. widely [1, 2]. In the process of motor optimization design, torque characteristics and noise characteristics are the two indexes that must be considered. The SPMSM with unequal magnetic poles structure has a smaller torque ripple than that of the equal magnetic poles structure. However, the noise characteristics of the motor become more complex. Besides, the rotor eccentricity, which arised from the manufacturing tolerances and other factors, will change the magnetic field and cause the motor vibration, noise, etc. [3]. Therefore, the magnetic field and noise characteristics of the rotor eccentric SPMSM with unequal pole structure should be investigated.

In general, the calculation methods of the magnetic field are mainly divided into finite element analysis (FEA) method and analytical method [4]. For a motor with a complex structure and nonlinear material, the FEA method is often adopted to calculate the magnetic field. However, it is time-consuming in magnetic field calculation. And, the relation between parameters and performances is difficult to understand. The analytical method is characterized by fast calculation speed and the explicit relationship between the structural parameters and performances. It will benefit the fast magnetic field calculation and the study of noise characteristics [5, 6].

*Correspondence: yushenbo@126.com

In [7–9], the magnetic field of rotor eccentric induction motor, synchronous reluctance motors, etc. are calculated using the winding function method analytically. However, since the tangential magnetic field is neglected, the winding function method cannot satisfy the calculation accuracy of SPMSM. In [10–12], the perturbation analysis (PA) method and subdomain method is applied to the analytical calculation of rotor eccentric SPMSM. Since the tangential magnetic field is calculated, the calculation accuracy of rotor eccentricity SPMSM is improved. However, the PA method and subdomain method is complicated in the process of modeling and solving [13]. In [14], with the characteristic of easily modeling, the conformal transformation (CT) method is applied to the analytic calculation of rotor eccentric SPMSM. However, the accuracy of calculation results should be improved in further study. In [15–17], the concept of magnetization surface current (MSC) and equivalent boundary method is applied to the analytic calculation of rotor eccentric SPMSM. It has the advantages of easily modeling and solving. Although much achievement has been made in the analytical modeling of rotor eccentric SPMSM, the modeling of rotor eccentric SPMSM with unequal magnetic poles structure is still an unsolved problem for the complication of the rotor structure.

The noise of PMSM contains electromagnetic noise, machinery noise, and aero-acoustics noise (will not be discussed) [18, 19]. The electromagnetic noise primarily arise from radial electromagnetic force. The radial electromagnetic force will affect the vibration displacement amplitude of the motor surface. Then, the electromagnetic noise characteristics will be generated. The mechanical noise is mainly caused by rotor dynamic unbalance, bearing, and other factors. Besides, the motor modal will also affect the vibration noise. When the natural frequency is coincident to radial electromagnetic force frequency, the amplitude of noise will be increased. The rotor eccentricity will change the stator radial electromagnetic force and rotor unbalanced electromagnetic force (UMF). Then, the noise characteristics of the motor will be changed. In [20, 21], the FEA method is used for studying the effect of rotor eccentricity on noise characteristics of SPMSM. And, in [22], the FEA method is used for studying the noise characteristics of rotor concentric SPMSM with unequal magnetic poles structure. However, there is no research about the noise characteristics of the rotor eccentric SPMSM with unequal magnetic poles structure.

In this paper, for the sake of predicting the magnetic field and studying the effect of rotor eccentricity on noise characteristics rapidly, an analytical model of rotor eccentric SPMSM with unequal magnetic poles structure is proposed. During the modeling process, the PM is replaced by ESC, and the effect on the air gap magnetic field, which arised from stator, is replaced by the CCS magnetic field. The current density Js of CCS is acquired with the method of equivalent boundary. Then, the comparison of the analytical results of the magnetic field and FEA results are made. At last, on the basis of the analytical model of the SPMSM, the effect on the electromagnetic force, which resulted from rotor eccentricity, is researched. Then, the effect on noise characteristics of rotor eccentricity is studied from the perspective of force source. Furthermore, the experiments of noise comparison are done to verify the effectiveness of noise characteristics research.

2. Analytical magnetic field model

2.1. Modeling process and assumptions

In this paper, an rotor eccentric 36-slot-8-pole SPMSM with unequal magnetic poles structure and closed slot armature is presented. The two-dimensional structure and schematic of rotor eccentric SPMSM with unequal magnetic poles structure are shown in Figures 1a and 1b, respectively. The rotor permanent magnet consists of a big magnetic pole and seven small magnetic poles. R_r and R_s are the radius of the rotor and inner surface of the stator, respectively. O_r and O_s are the center of the rotor and stator, respectively. h_m is the thickness

of the permanent magnet. a_n is the eccentric distance. The structure size of big and small magnetic poles is shown in Figure 2.

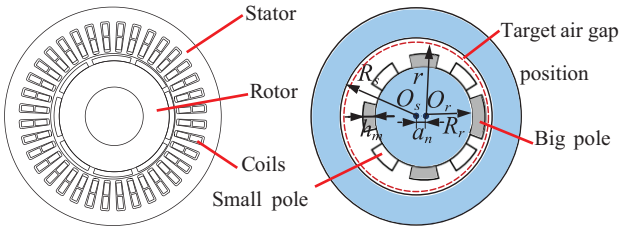

Figure 1. The two-dimensional structure and schematic of rotor eccentric SPMSM with unequal magnetic poles structure.

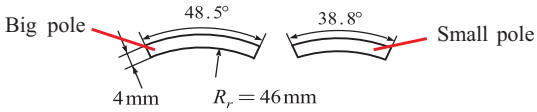

Figure 2. The structure size of big and small magnetic pole.

The schematic diagram of no-load equivalent eccentric motor is shown in figure 3. The stator is replaced with CCS. The contour S and Ob are the stator inner surface of the original motor and the target air gap position, respectively. According to [23], the magnetic field of the equivalent motor between the rotor surface and contour S is consistent with that of the original motor. At the target position Ob, by superimposing the magnetic field of rotor permanent magnet and CCS, the air gap magnetic field is obtained. The equivalent motor model in Figure 3 is divided into the rotor permanent magnet model and CCS model, as shown in Figure 4.

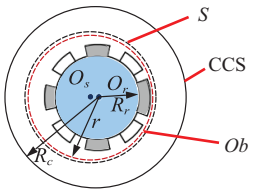

Figure 3. The schematic of no-load equivalent eccentric motor.

The detailed modeling process of the air gap magnetic field is represented as follows: (1) In Figure 4a, the CCS is removed, and based on the ESC method, a rotor permanent magnetic field model is established. (2) In Figure 4b, the permanent magnets are removed, the CCS magnetic field model is built, and the current density Js is acquired. Then, the analytical model of no-load motor is obtained using the superposition method. (3) The armature winding magnetic field model is established without considering the effects of rotor eccentricity. Then, by superimposing the magnetic field of no-load motor and the armature winding, the analytical model of on-load motor is obtained.

Besides, during the modeling process, some necessary assumptions are made and expressed as follows: (1) The leakage flux is ignored. (2) The permeability of cores is infinite. (3) The end effects are ignored. (4)

The effects of rotor eccentricity are ignored in the armature winding magnetic field model.

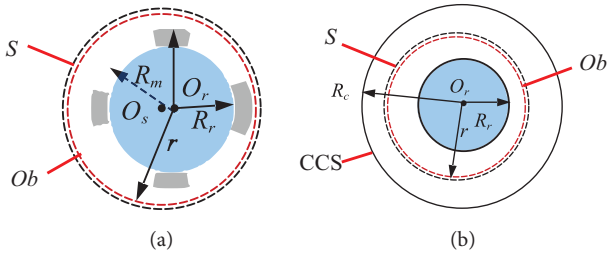

Figure 4. The rotor permanent magnet model and the CCS model.

2.2. Magnetic field modeling of rotor permanent magnet

Since the structural parameters of each permanent magnet are unequal, it is difficult to make use of a unified formula to express the magnetization of the permanent magnets. Therefore, the modeling process becomes relatively complicated. In order to realize the calculation of rotor permanent magnet magnetic field, the magnetic field of a single PM is replaced by that of ESC which is distributed on the surface of the PM. And, by superimposing the magnetic field of all permanent magnets, the rotor permanent magnet magnetic field is acquired.

In the O_r coordinates, the rotor permanent magnet model in Figure 4a is divided into two regions.

Region 1: PM $R_r \leq r \leq R_m$

Region 2: Air $R_m \leq r$

where $R_m = R_r + h_m$ is an external edge radius of PM.

The structural parameters of the PM and the distribution of ESC microelement are shown in Figure 5. $2\eta_i$ and δ_i are the opening angle of the PM and magnetic pole, respectively. Then, the magnetic field of a single PM (parallel magnetization) is obtained by integrating the magnetic field of the ESC microelement.

A single-turn coil in region 1 is shown in Figure 6. E and F are both sides of the coil. a is the radius of the concentric circle where the coil is located.

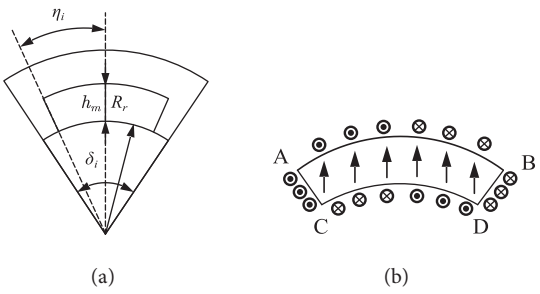

Figure 5. The structural parameters of PM and the distribution of ESC microelement.

The vector magnetic potential A_{z1} generated by a single-turn coil in region 2 can be expressed as

$$A_{z1} = \sum_{m=1}^{\infty} \frac{\mu_0 i}{m\pi} r^{-m}(a^m + a^{-m}R_r^{2m}) \sin m\zeta \sin m\theta. \quad (1)$$

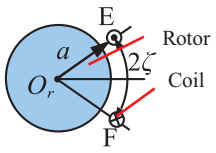

Figure 6. The single-turn coil in region 1.

In polar coordinates, the radial and tangential magnetic flux densities in air gap are represented as (the radial and tangential magnetic flux density are the flux density component of the air gap magnetic field along the radial and tangential direction, respectively)

$$Br_1(r,\theta) = \frac{1}{r}\frac{\partial A_z}{\partial \theta} = \sum_{m=1}^{\infty} \frac{\mu_0 i}{\pi} r^{-m-1}(a^m + a^{-m}R_r^{2m}) \sin m\zeta \cos m\theta \ , \tag{2}$$

$$Bt_1(r,\theta) = -\frac{\partial A_z}{\partial r} = -\sum_{m=1}^{\infty} \frac{\mu_0 i}{\pi} r^{-m-1}(a^m + a^{-m}R_r^{2m}) \sin m\zeta \sin m\theta \ . \tag{3}$$

The directions of the ESC microelement on AC and BD are the opposite. The ESC microelement is $di = J_1 da$, and the current density $J_1 = H_{cb}\cos\eta_i$ (H_{cb} is the coercivity). By replacing the current i in Equations (2) and (3) with di, and integrating a, the radial and tangential resultant magnetic flux densities, which is generated by ESC that are located on AC and BD, in air gap can be expressed as follows:

$$Br_{ABCDi}(r,\theta) = \frac{\mu_0 H_{cb}\cos\eta_i}{\pi} \sum_{m=1}^{\infty} r^{-m-1} K_{m1} \sin m\eta_i \cos(m(\theta-\alpha_i)) \tag{4}$$

$$Bt_{ABCDi}(r,\theta) = -\frac{\mu_0 H_{cb}\cos\eta_i}{\pi} \sum_{m=1}^{\infty} r^{-m-1} K_{m1} \sin m\eta_i \sin(m(\theta-\alpha_i)), \tag{5}$$

where μ_0 is vacuum permeability, α_i is the angle between permanent magnet axis and polar axis, and K_{m1} can be expressed as

$$K_{m1} = \begin{cases} \frac{(R_r+h_m)^{m+1}-R_r^{m+1}}{m+1} + R_r^{2m}\ln\frac{R_r+h_m}{R_r} & m=1 \\ \frac{(R_r+h_m)^{m+1}-R_r^{m+1}}{m+1} + R_r^{2m}\frac{(R_r+h_m)^{-m+1}-R_r^{-m+1}}{1-m} & m\neq 1 \end{cases}$$

The ESC microelement on the arc AB and CD is $di = rJ_2 d\theta$, and the current density $J_2 = H_{cb}\sin\theta_{\eta i}$. By replacing the current i in equations (2) and (3) with di, and integrating θ, the radial and tangential magnetic flux densities, which is generated by ESC that are located on arc AB and CD, in air gap can be expressed as follows:

$$Br_{ABi}(r,\theta) = \frac{\mu_0 H_{cb}}{\pi} K_{m2}\cos(m(\theta-\alpha_i)) \sum_{m=1}^{\infty} \frac{(R_r+h_m)^{m+1} + (R_r+h_m)^{-m+1}R_r^{2m}}{r^{m+1}} \tag{6}$$

$$Bt_{ABi}(r,\theta) = -\frac{\mu_0 H_{cb}}{\pi} K_{m2}\sin(m(\theta-\alpha_i)) \sum_{m=1}^{\infty} \frac{(R_r+h_m)^{m+1} + (R_r+h_m)^{-m+1}R_r^{2m}}{r^{m+1}} \tag{7}$$

$$Br_{CDi}(r,\theta) = -\frac{2\mu_0 H_{cb}}{\pi}\sum_{m=1}^{\infty}\left(\frac{Rr}{r}\right)^{m+1} K_{m2}\cos(m(\theta-\alpha_i)) \tag{8}$$

$$Bt_{CDi}(r,\theta) = \frac{2\mu_0 H_{cb}}{\pi}\sum_{m=1}^{\infty}\left(\frac{Rr}{r}\right)^{m+1} K_{m2}\sin(m(\theta-\alpha_i)), \tag{9}$$

where K_{m2} can be expressed as

$$K_{m2} = \begin{cases} \frac{1}{2}\eta_i - \frac{1}{4}\sin 2\eta_i & m = 1 \\ \frac{1}{2(m-1)}\sin(m-1)\eta_i - \frac{1}{2(m+1)}\sin(m+1)\eta_i & m \neq 1 \end{cases}$$

According to Equations (4)–(9), the radial and tangential magnetic flux densities, which are generated by the rotor permanent magnets of the SPMSM with unequal magnetic poles structure (pole pairs is p), in air gap can be expressed as follows:

$$Br_{PM}(r,\theta) = \sum_{i=1}^{2p}[Br_{ABCDi}(r,\theta) + Br_{ABi}(r,\theta) + Br_{CDi}(r,\theta)], \tag{10}$$

$$Bt_{PM}(r,\theta) = \sum_{i=1}^{2p}[Bt_{ABCDi}(r,\theta) + Bt_{ABi}(r,\theta) + Bt_{CDi}(r,\theta)]. \tag{11}$$

2.3. Magnetic field modeling of CCS

In this section, the CCS magnetic field model is built, and the current density Js is acquired. Then, the magnetic field, which is generated by a rotor eccentric no-load SPMSM with unequal magnetic poles structure, is obtained.

In the O_r coordinate system, the CCS model in Figure 4b is divided into two regions.

Region 3: $R_r \leq r \leq R_c$

Region 4: $R_c \leq r$

where $R_c = a_n + R_s$ is the radius of the concentric circle of CCS.

The Fourier series of Js is represented by

$$Js(\theta) = \sum_{m=1}^{\infty} J_{sc}\cos m\theta + J_{ss}\sin m\theta, \tag{12}$$

where J_{sc} and J_{ss} are the cosine and sine coefficients of Js, respectively.

The vector magnetic potentials of Js, which is located in regions 3, can be expressed as

$$A_{z3} = \sum_{m=1}^{\infty}\frac{\mu_0(r^m - {R_r}^{2m}r^{-m})}{2Rc^{-m-1}}(J_{sc}\cos m\theta + J_{ss}\sin m\theta). \tag{13}$$

According to Equation (13), in regions 3, the radial and tangential magnetic flux density, which is generated by Js, in air gap are represented as follows:

$$Br_{3-ESCJs}(r,\theta) = \sum_{m=1}^{\infty}\frac{\mu_0(r^{m-1} + {R_r}^{2m}r^{-m-1})}{2Rc^{-m-1}}(J_{sc}\sin m\theta - J_{ss}\cos m\theta), \tag{14}$$

$$Bt_{3-ESCJs}(r,\theta)=\sum_{m=1}^{\infty}\frac{-\mu_0(r^{m-1}-{R_r}^{2m}r^{-m-1})}{2Rc^{-m-1}}(J_{sc}\cos m\theta+J_{ss}\sin m\theta). \tag{15}$$

According to the equivalent boundary method, at the contour S, the tangential magnetic flux density should be zero. Therefore, the tangential magnetic field of CCS must offset that of rotor permanent magnet. Then, the tangential magnetic flux density, which is located at the contour S, should be satisfied with the following equation.

$$Bt_3|_S=Bt_{PM}|_S+Bt_{3-ESCJs}|_S=0 \tag{16}$$

The Fourier series of Bt_{PM}, which is located at the contour S, is represented as

$$Bt_{PM}|_S(\theta)=\sum_{m=1}^{\infty}Bt_{PMSC}\cos m\theta+Bt_{PMSS}\sin m\theta, \tag{17}$$

where Bt_{PMSC} and Bt_{PMSS} are the cosine and sine coefficients of $Bt_{PM}|_S$, respectively.

Then, the following equation can be obtained.

$$\sum_{m=1}^{\infty}Bt_{PMSC}\cos m\theta+Bt_{PMSS}\sin m\theta=\sum_{m=1}^{\infty}\frac{\mu_0(r^{m-1}-R_r r^{-m-1})}{2Rc^{-m-1}}(J_{ss}\sin m\theta+J_{sc}\cos m\theta) \tag{18}$$

And, according to Equations (12) and (18), current density Js of CCS can be represented as

$$Js(\theta)=\sum_{m=1}^{\infty}\frac{2Rc^{-m-1}}{\mu_0(r^{m-1}-R_r^{2m}r^{-m-1})}(Bt_{PMSC}\cos m\theta+Bt_{PMSS}\sin m\theta). \tag{19}$$

Therefore, the cosine and sine coefficients of Js in equation (12) can be calculated.

Based on equations (10), (11), (14) and (15), the radial and tangential magnetic fields, which are generated by no-load motor, in air gap are represented as follows:

$$Br_3(r,\theta)=Br_{PM}(r,\theta)+Br_{3-ESCJs}(r,\theta), \tag{20}$$

$$Bt_3(r,\theta)=Bt_{PM}(r,\theta)+Bt_{3-ESCJs}(r,\theta). \tag{21}$$

2.4. Magnetic field modeling of armature winding

Since the magnetic flux densities amplitude of armature winding for SPMSM is smaller than that of the rotor, it can be assumed that rotor eccentricity does not affect the armature winding magnetic field. Thus, the simplified magnetic field modeling of armature winding can be realized.

During the modeling process, the magnetic field of armature winding is replaced by that of current sheet located on the stator inner surface. The current density of the current sheet is represented as follows:

$$J(t)=\begin{cases}\frac{Nsi(t)}{a_s w_s} & a_y-\frac{\alpha_0}{2}\le\theta\le a_y+\frac{\alpha_0}{2}\\ -\frac{Nsi(t)}{a_s w_s} & -a_y-\frac{\alpha_0}{2}\le\theta\le -a_y+\frac{\alpha_0}{2}\\ 0 & others\end{cases} \tag{22}$$

where Ns is the turns of the coil, a_s is the number of parallel branches, w_s is the width of stator slot, $2a_y$ is the span angle of a single-turn coil, and α_0 is the opening angle of the slot.

According to [24], the radial and tangential magnetic fields, which is produced by a single-turn coil that is located on the stator inner surface, in air gap are represented as follows:

$$Br_{coil} = \frac{\mu_0 i}{\pi r} \sum_{m=1}^{\infty} \frac{R_r^m}{R_s^m} \left(\frac{{R_s}^{2m} + {R_r}^{2m}}{{R_s}^{2m} - {R_r}^{2m}} \right) \left(\frac{r^m}{R_r^m} + \frac{R_r^m}{r^m} \right) \sin(ma_y) \cos(m\theta), \tag{23}$$

$$Bt_{coil} = -\frac{\mu_0 i}{\pi r} \sum_{m=1}^{\infty} \frac{R_r^m}{R_s^m} \left(\frac{{R_s}^{2m} + {R_r}^{2m}}{{R_s}^{2m} - {R_r}^{2m}} \right) \left(\frac{r^m}{R_r^m} - \frac{R_r^m}{r^m} \right) \sin(ma_y) \sin(m\theta). \tag{24}$$

According to Equations (22)–(24), the radial and tangential magnetic flux density, which is produced by A phase winding, in air gap are obtained by using the superposition principle and expressed as follows:

$$\begin{aligned} Br_A(r,\theta,t) = \tfrac{2\mu_0 R_s J(t)}{\pi r} \sum_{k=0}^{2pc-1} \sum_{n=1}^{q} \sum_{m=1}^{\infty} \tfrac{1}{m} \left(\tfrac{R_r}{R_s} \right)^m \left(\tfrac{R_s^{2m} + R_r^{2m}}{R_s^{2m} - R_r^{2m}} \right) \left(\tfrac{r^m}{R_s^m} + \tfrac{R_s^m}{r^m} \right) \\ \sin\left(mp\tfrac{\alpha_0}{2}\right) \sin\left(mpa_y\right) \cos[mp(\theta - \tfrac{2n-q-1}{2}\alpha_t + k\tfrac{\pi}{pc})], \end{aligned} \tag{25}$$

$$\begin{aligned} Bt_A(r,\theta,t) = -\tfrac{2\mu_0 R_s J(t)}{\pi r} \sum_{k=0}^{2pc-1} \sum_{n=1}^{q} \sum_{m=1}^{\infty} \tfrac{1}{m} \left(\tfrac{R_r}{R_s} \right)^m \left(\tfrac{R_s^{2m} + R_r^{2m}}{R_s^{2m} - R_r^{2m}} \right) \left(\tfrac{r^m}{R_s^m} - \tfrac{R_s^m}{r^m} \right) \\ \sin\left(mp\tfrac{\alpha_0}{2}\right) \sin\left(mpa_y\right) \sin[mp(\theta - \tfrac{2n-q-1}{2}\alpha_t + k\tfrac{\pi}{pc})], \end{aligned} \tag{26}$$

where $2pc$ is the number of coils assembly, q is the number of the coils, π/pc is the angle of adjacent coils, α_t is the slot pitch angle.

Similarly, the radial and tangential magnetic flux densities, which are produced by the B and C phase windings, in air gap are obtained and expressed as $Br_B(r,\theta)$, $Bt_B(r,\theta)$, $Br_C(r,\theta)$, and $Bt_C(r,\theta)$, respectively. The radial and tangential magnetic fields, which are generated by armature winding, in air gap are represented as follows:

$$Br_4(r,\theta) = Br_A(r,\theta) + Br_B(r,\theta) + Br_C(r,\theta) \tag{27}$$

$$Bt_4(r,\theta) = Bt_A(r,\theta) + Bt_B(r,\theta) + Bt_C(r,\theta) \tag{28}$$

According to Equations (20), (21), (27), and (28), the radial and magnetic fields, which are generated by on-load motor, in air gap are represented as follows:

$$Br(r,\theta) = Br_3(r,\theta) + Br_4(r,\theta), \tag{29}$$

$$Bt(r,\theta) = Bt_3(r,\theta) + Bt_4(r,\theta). \tag{30}$$

3. FEM validation

In this section, the ANSYS software was used in FEM validation. It is used to calculate the air gap magnetic field of the motor. The parameters of the motor are shown in Table 1.

According to Equations (20) and (21), the radial and tangential magnetic flux density of no-load motor are acquired at the target air gap position $r = (R_s + R_r + h_m)/2$, as shown in Figures 7a and 7b, respectively.

Table 1. The parameters of motor.

Items	Values
Rated speed / r/min	2000
Outer radius / mm	92
The radius of stator inner surface R_s s/ mm	52
The radius of rotor outer surface R_r / mm	46
The thickness of PM h_m / mm	4
Stator axial length / mm	150
Pole pairs	4
Number of slots	36
Number of phases	3

At this point, the rotation angle of the rotor is 0°, the rotor rotation center position O_r of the rotor is (0.8, 0°) in the O_s coordinate system, and the relative position of rotor is shown in figure 1b. The analytical results of air gap flux density are almost identical to the FEA results. Because of rotor eccentricity, the maximum value of the air-gap flux density is decreased at the position with a large air gap and increased at the position with a small air gap. Besides, due to the unequal magnetic poles structure, the residual magnetization of the big magnetic pole is lesser than that of the small magnetic pole. This will lead to the air gap flux density at the small magnetic pole is bigger than that at the big magnetic pole for the rotor concentric SPMSM with unequal magnetic poles structure.

According to Equations (27) and (28), the radial and tangential magnetic flux density generated by armature winding are acquired at the target air gap position r= (R_s+ R_r+ h_m)/2, and shown in Figures 8a and 8b, respectively. The analytical results of air gap flux density of the motor without rotor eccentricity is nearly consistent with the FEM results of the motor with rotor eccentricity. Then, the assumption that rotor eccentricity does not affect the armature winding magnetic field is confirmed.

According to Equations (29) and (30), the radial and tangential magnetic flux density of on-load motor are acquired at the target air gap position r= (R_s+ R_r+ h_m)/2, as shown in Figures 9a and 9b, respectively. At this point, the rotation angle of the rotor is 0°, the rotor rotation center position O_r of the rotor is (0.8, 0°) in the O_s coordinate system, and the relative position rotor is shown in Figure 1b. The analytical results of air gap flux density are almost identical to the FEA results. Under the action of rotor eccentricity, the variation trend of on-load motor magnetic field is nearly consistent with that of no-load motor magnetic field.

4. Noise characteristics

Since, at any frequency, the increase of radical electromagnetic force of the stator will increase the electromagnetic noise of the motor and the converse is also true. At the rotating frequency, the increase of the unbalanced electromagnetic force (UMF) of the rotor will increase the mechanical noise and the converse is also true. Therefore, the effect of rotor eccentricity on noise characteristics can be studied from the perspective of force source. In this section, firstly, the effect on electromagnetic force and electromagnetic force waves, which arised from rotor eccentricity, are analyzed. Then, the frequencies of motor noise with a significant variation, which is caused by rotor eccentricity, are obtained. The effect of rotor eccentricity on the electromagnetic noise is studied based on the analytical model. Secondly, the effect on the UMF of the rotor, which arised from rotor

eccentricity, is analyzed. The effect of rotor eccentricity on mechanical noise is studied based on the analytical model. Finally, based on the noise contrast test, the effectiveness of theoretical research on noise characteristics are verified. Then, the analytical model of rotor eccentric SPMSM with unequal magnetic poles structure is further verified.

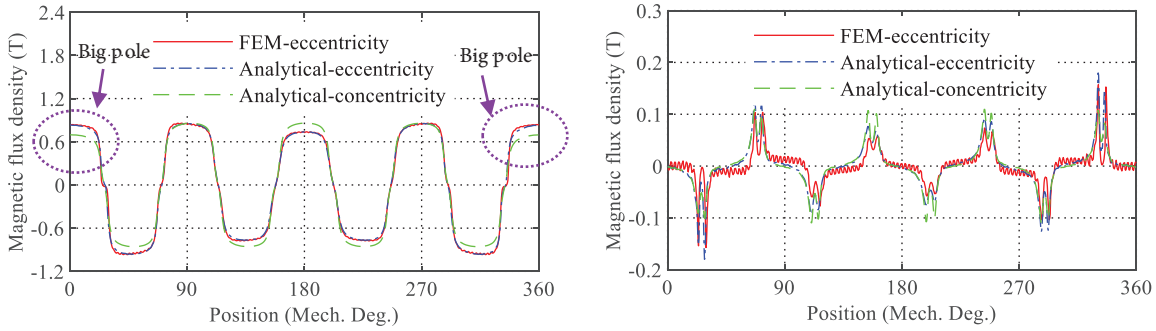

Figure 7. The radial and tangential magnetic flux density of no-load motor.

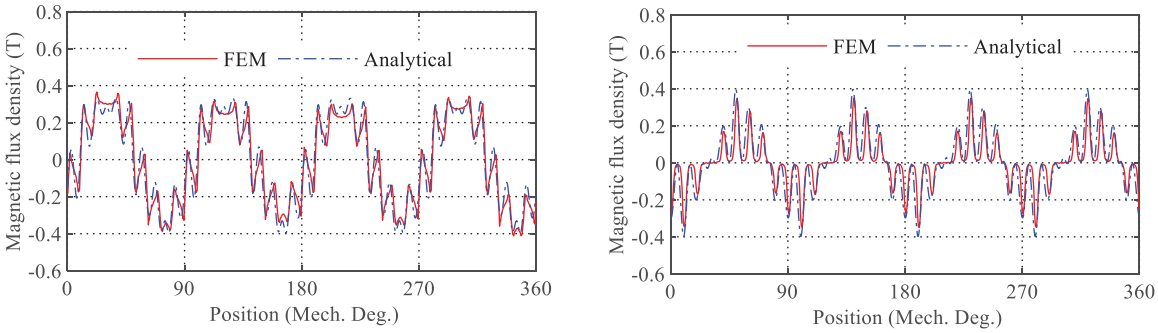

Figure 8. The radial and tangential magnetic flux density of armature winding.

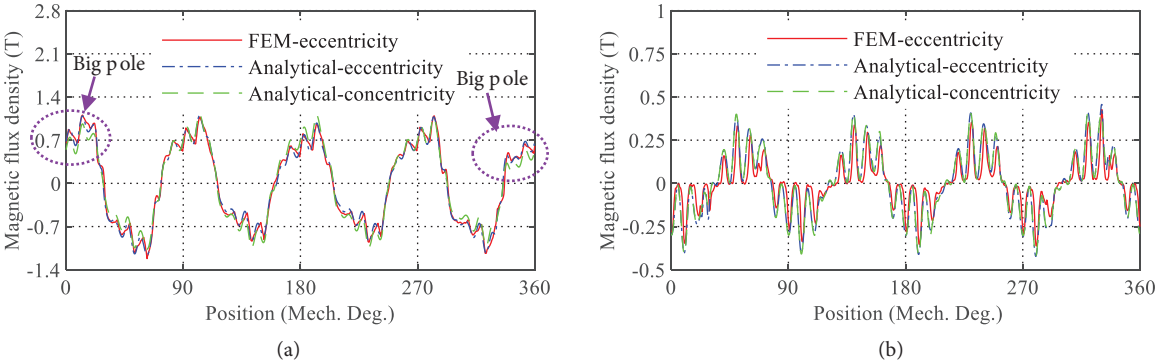

Figure 9. The radial and tangential magnetic flux density of on-load motor.

4.1. The effect of rotor eccentricity on electromagnetic noise

The current of PWM inverter can be divided into two parts: sinusoidal waveform current and harmonics current. In general, the harmonic current frequency is near the integer multiples of inverter switching frequency. And, the harmonics amplitude of rotor magnetic field in the high frequency are small. Besides, the effect on armature winding magnetic field, which is arised from the rotor eccentricity, is ignored in the analytical model. Therefore, when studying the effect of rotor eccentricity on electromagnetic noise, only the low-frequency electromagnetic force should be investigated.

Since the tangential magnetic field on the stator inner surface is zero, the tangential component of electromagnetic force density (tangential electromagnetic force density) is zero. Then, the electromagnetic force density at a fixed position of the stator inner surface is equal to the radial component of electromagnetic force density (radial electromagnetic force density) and can be represented as

$$f_r(\theta,t)=\frac{Br^2(\theta,t)}{2\mu_0}. \tag{31}$$

According to [25], when neglecting the harmonics current of PWM inverter, the electromagnetic force wave, which is along the circumference of the stator inner surface, is represented as

$$f_r(\theta,t)=\frac{1}{2\mu_0}\sum_{v}^{\infty}\sum_{u}^{\infty}Br_vBr_u\cos\left[(v\pm u)\theta-(\nu/p\pm1)\omega_0t-\varphi_{vu}\right], \tag{32}$$

where Br_v and Br_u are the v order and u order harmonic amplitude of magnetic field generated by permanent magnet magnetic and armature winding in air gap, respectively. $|v\pm u|$ is the electromagnetic force wave order. $(v/p\pm1)\omega_0$ and ω_0 are the frequency of electromagnetic force wave and the fundamental magnetic field, respectively.

On the base of analytical calculation, the harmonics of electromagnetic force density generated by the on-load rotor eccentricity motor at a fixed point of the stator inner surface is shown in Figure 10. For the static eccentric motor, the rotor rotation center does not coincide with the stator circle center, and the rotation center remains unchanged. For the dynamic eccentric motor, the rotor rotation center does not coincide with the stator circle center, and the rotor rotation center rotates around the stator circle center. "Dynamic eccentricity-1" is the dynamic eccentricity with a small air gap length at the big magnetic pole. "Dynamic eccentricity-2" is a dynamic eccentricity with a small air gap length at a small magnetic pole which is 180 degrees away from the big magnetic pole. It can be seen that the 1st order and $(2pk\pm1)$th (k=1,2,3, 4…) order harmonics amplitude of electromagnetic force density are changed obviously. The detailed description of the changes are as follows:

(1) The 1st order harmonics amplitude of electromagnetic force density is increased in static and dynamic eccentricity motor (the frequency is 33.3 Hz). Under the situation of same eccentric distance, the electromagnetic force density amplitude of the "dynamic eccentricity-2" motor is the biggest, followed by that of static eccentricity motor. That of "dynamic eccentricity-1" motor is the smallest.

(2) The $(2pk$-1)th order harmonics amplitude of electromagnetic force density are increased in static eccentricity and "dynamic eccentricity-1" motor, and decreased in "dynamic eccentricity-2" motor. In the case of the same eccentric distance, the electromagnetic force density amplitude of the "dynamic eccentricity-1" motor is the biggest, followed by that of static eccentricity motor. That of "dynamic eccentricity-2" motor is the smallest. The $(2pk$-1)th order harmonics frequency of electromagnetic force density is $(2pk$-1$)\omega_0/p$, such as 233.1, 499.5, 765.9, 1032.3 Hz, etc.

(3) The $(2pk+1)$th order harmonics amplitude of electromagnetic force density are increased in static eccentricity and "dynamic eccentricity-2" motor, and decreased in "dynamic eccentricity-1" motor. In the case of the same eccentric distance, the electromagnetic force density amplitude of the "dynamic eccentricity-2" motor is the biggest, followed by that of static eccentricity motor. That of "dynamic eccentricity-1" motor is the smallest. The $(2pk+1)$th order harmonics frequency of electromagnetic force density is $(2pk+1)\omega_0/p$, such as 299.7, 566.1, 832.5, 1098.9 Hz, etc.

Since the effect of rotor eccentricity on the armature winding magnetic field is neglected, the effect of rotor eccentricity on the electromagnetic force wave of on-load motor can be studied just by analyzing the harmonics amplitude of rotor magnetic field. Based on the analytical model, the harmonics magnetic field of rotor is shown in figure 11. According to Equation (32) and Figure 11, it can be seen that the $((2k\text{-}1)p\pm1)$th (k=1, 2, 3, 4…) order harmonics amplitude of the rotor magnetic field are changed obviously. The specific changes are described as follows:

(1) In the case of $v=(2k\text{-}1)p\text{-}1$, the static eccentricity and "dynamic eccentricity-1" increases the harmonics amplitude of rotor magnetic field, and the "dynamic eccentricity-2" decreases the harmonics amplitude of rotor magnetic field. Therefore, at the frequencies of $(v/p\pm1)\omega_0$ Hz, such as 233.1, 499.5, 765.9, 1032.3 Hz, etc., the electromagnetic force wave amplitude of the motor with static eccentricity or "dynamic eccentricity-1" is increased, and that of "dynamic eccentricity-2" is decreased. Besides, in the case of same eccentric distance, the electromagnetic force wave amplitude of the "dynamic eccentricity-1" motor is the biggest, followed by that of static eccentricity motor, and that of "dynamic eccentricity-2" motor is the smallest.

(2) In the case of $v=(2k\text{-}1)p+1$, the static eccentricity and "dynamic eccentricity-2" increases the harmonics amplitude of rotor magnetic field, and the "Dynamic eccentricity-1" decreases the harmonics amplitude of rotor magnetic field. Therefore, at the frequencies of $(v/p\pm1)\omega_0$ Hz, such as 33.3, 299.7, 566.1, 832.5, 1098.9 Hz, etc., the electromagnetic force wave amplitude of the motor with static eccentricity or "dynamic eccentricity-2" is increased, and that of "dynamic eccentricity-1" is decreased. Besides, in the case of same eccentric distance, the electromagnetic force wave amplitude of the "dynamic eccentricity-2" motor is the biggest, followed by that of static eccentricity motor, and that of "dynamic eccentricity-1" motor is the smallest.

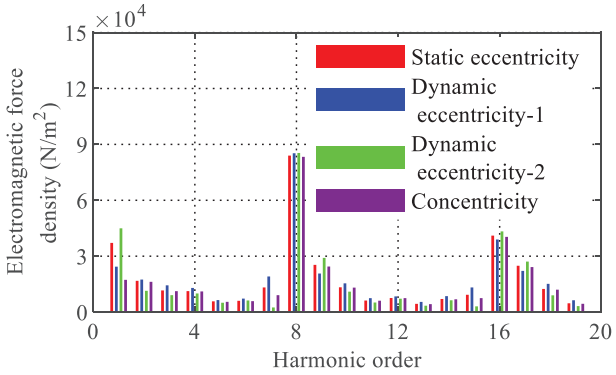

Figure 10. The harmonic of electromagnetic force density.

In conclusion, the effect on the electromagnetic force, which arised from rotor eccentricity, at a fixed point is nearly consistent with that of electromagnetic force wave amplitude along the stator inner surface. At the frequencies, which the amplitudes of electromagnetic force and electromagnetic force waves are increased, the amplitude of electromagnetic noise will be increased. And, the converse is also true. Then, the frequencies

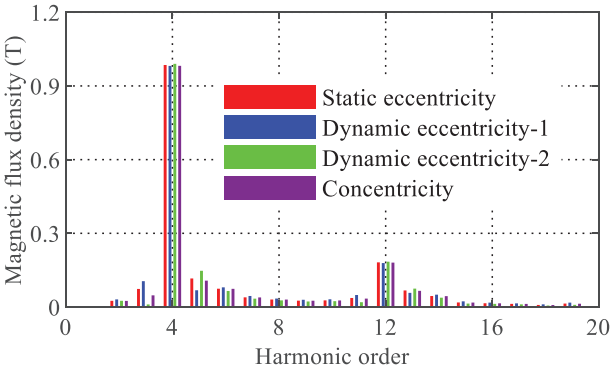

Figure 11. The harmonics magnetic field of rotor.

of motor noise with a significant variation, which is caused by rotor eccentricity, are obtained. The effect of rotor eccentricity on the electromagnetic noise is studied based on the analytical model.

4.2. The effect of rotor eccentricity on mechanical noise.

Eccentricity will affect the UMF of the rotor, which will further affect the mechanical noise characteristics of the motor. The frequency of mechanical noise is the rotation frequency and its integer multiples.

The x and y component of rotor UMF are expressed as

$$F_x = \frac{rL_s}{2\mu_0}\int_0^{2\pi}[(Bt^2 - Br^2)\cos\theta + 2BrBt\sin\theta]d\theta, \tag{33}$$

$$F_{\mathrm{y}} = \frac{rL_s}{2\mu_0}\int_0^{2\pi}[(Bt^2 - Br^2)\sin\theta - 2BrBt\cos\theta]d\theta, \tag{34}$$

where L_s is the length of the stator.

The resultant force of the UMF is represented as

$$F_{UMF} = \sqrt{F_x^2 + F_y^2}. \tag{35}$$

In the case of the same eccentric distance, the component of UMF in the y-direction change with that of in the x-direction is shown in Figure 12. For the static eccentric motor, the amplitude of UMF changes significantly. The average amplitude of the UMF of the "dynamic eccentricity -2" motor is the biggest. The average amplitude of UMF of the concentric motor is the smallest. Besides, according to the magnetic field distribution in air gap, the resultant force of UMF always points to the small magnetic pole which is 180 degrees away from the big magnetic pole for motor without eccentricity. Therefore, under the action of UMF, the concentric motor would become a motor with "dynamic eccentricity-2". Then, the noise characteristics of the motor would be changed.

The harmonics of the UMF are shown in Figure 13. The harmonics amplitude of rotor UMF is almost unaffected by dynamic eccentricity. However, static eccentricity produces new kinds of harmonics of UMF. Among these harmonics, the amplitude of 1st harmonic is the biggest. It will increase the amplitude of the mechanical noise in the rotational frequency (33.3 Hz).

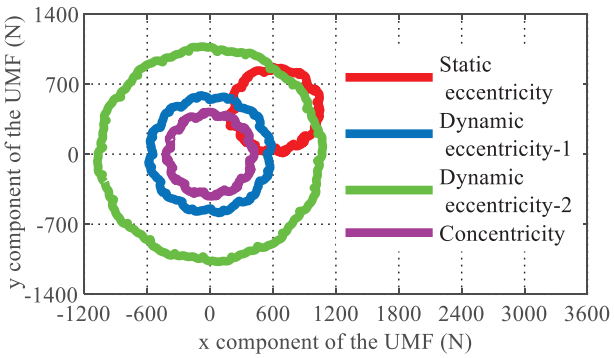

Figure 12. The component of UMF in the y-direction change with that of in the x-direction.

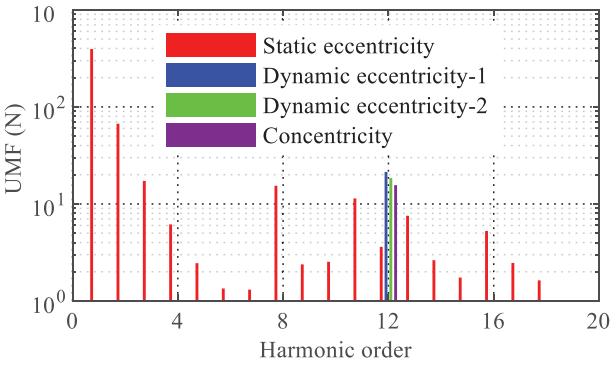

Figure 13. The harmonics of UMF.

4.3. Experiments and discussion

In this section, taking the static eccentricity as an example, the effectiveness of noise characteristics research is verified. The motor-1 is the SPMSM with rotor static eccentricity and unequal magnetic poles (ignoring the small stator slot effects). By improving the manufacturing technique of motor-1, the rotor static eccentricity of motor-1 is removed, and the motor-2 is obtained. Then, the sound pressure level (SPL) of motor-1 and motor-2 are measured, respectively. And, the results of experiments are discussed.

The schematic diagram of motor noise measurement and the test site is shown in Figures 14 and 15, respectively. The test equipment includes the motor, shaft coupling, CZ magnetic powder brake, sound pressure meter, B&K3050-A-060 data collector, MD290 AC drive system (the control algorithm is vector control), and upper computer. The CZ magnetic powder brake is used for providing load torque for the motor. The noise information is collected by sound pressure meter. The SPL frequency spectrum of on-load motor-1 and motor-2 are shown in Figures 16a and 16b (the horizontal axis represents the frequency of SPL frequency spectrum), respectively. It can be seen that the SPL of motor-1 and motor-2 are prominent at low frequency, and the difference between them is noticeable. And, the SPL of motor-1 and motor-2 at the middle and high frequency is small, and the difference between them is not apparent. Therefore, when analyzing the effect of rotor eccentricity on electromagnetic noise, only the low-frequency noise should be investigated. Based on experimental results, at the frequency that static eccentricity has a great influence on the electromagnetic force, the SPL of two motors is compared and shown in Table 2 (the variation trend is the SPL variation trend of motor-2 relative to that

of motor-1). At the frequencies of 32, 240, 304, 496, 560, and 768 Hz, the noise amplitude of motor-1 is bigger than that of motor-2. At the frequencies of 832 and 1104 Hz, the noise amplitude of motor-2 is bigger than that of motor-1. And, at the frequencies of 1024 Hz, the noise amplitude of the two motors are nearly the same.

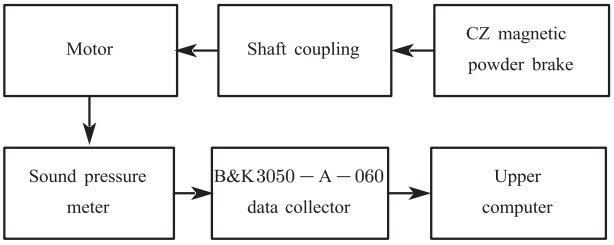

Figure 14. The schematic diagram of motor noise measurement.

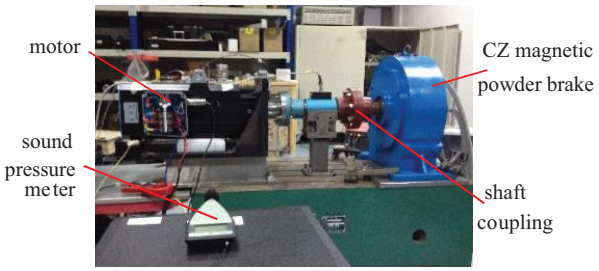

Figure 15. The test site of motor noise measurement.

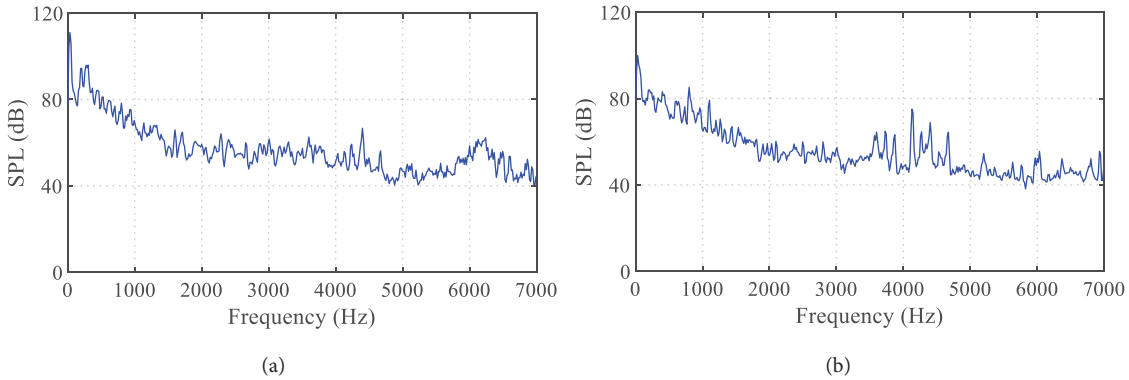

Figure 16. The SPL frequency spectrum of on-load motor-1 and motor-2.

Based on the theoretical analysis of the effect of static eccentricity, "dynamic eccentricity-2" and UMF on the noise characteristics of the motor, the reason for the changes of the SPL can be deduced as follows: (1) Due to the improvement of manufacturing technology, the static eccentricity of motor-2 is removed. Therefore, at the frequencies of 32, 240, 304, 496, 560, and 768 Hz, the amplitude of electromagnetic noise is decreased. (2) Due to the unequal magnetic poles structure, the concentric motor will also produce the UMF. Furthermore, under the action of the UMF, the concentric motor would become a motor with small "dynamic eccentricity-2". Therefore, at the frequencies of 832 and 1104 Hz, the amplitude of electromagnetic noise is increased. However,

Table 2. The comparison of SPL.

Theoretical value (Hz)	Measured value (Hz)	Motor-1 (dB)	Motor-2 (dB)	Variation trend
33.3	32	111	99.92	↓
233.1	240	85.85	82.92	↓
299.7	304	95.87	73.64	↓
499.5	496	76.57	73.1	↓
566.1	560	75.65	70.79	↓
765.9	768	74.39	68.17	↓
832.5	832	66.77	78.33	↑
1032.3	1024	66.11	66.54	↑
1098.9	1104	61.01	79.15	↑

at the frequency of 1024 Hz, the amplitude of electromagnetic noise is little changed, which may be caused by experimental errors. (3) Due to the rotation frequency of the motor is 33.3 Hz, at the frequency of 32 Hz, the noise contains the component of mechanical noise. Therefore, at 32 Hz, the decrease of UMF is partly responsible for the decrease of the noise amplitude.

Therefore, the effectiveness of noise characteristics research is verified by the experiments.

5. Conclusion

On the base of ESC method of permanent magnet and equivalent boundary method, an analytical model of rotor eccentricity SPMSM with unequal magnetic poles structure is proposed. Then, the rapid calculation of magnetic fields is realized. And, according to the analytical model, the effect on noise characteristics of the motor, which arised from rotor eccentricity, is researched rapidly from the perspective of force source.

The analytical results and FEA results of air gap flux density are nearly the same. The validity of the analytical model is confirmed. The calculation accuracy of the air gap magnetic field is satisfied. According to the analytical model, the frequencies of motor noise with a significant variation, which is caused by rotor eccentricity, are obtained. The effect of rotor eccentricity on the noise characteristics is studied. Besides, The noise comparison experiments are done. The SPL variation trend of analytical results is consistent with that of the experiment results. The effectiveness of the noise characteristic research is validated, and the effectiveness of analytical model of the motor is verified furtherly. Due to the space limitation, the content of motor performance parameters such as power, torque, speed, currents and magnetic flux densities in cores will be published in future papers.

Acknowledgment

This work was supported in part by the Natural Science Foundation of China under Grant 51175350, in part by the Science and Technology Project Program of Shenyang under Grant F15-199-1-13.

References

[1] Yang YB, Wang XH, Zhang R, Ding TT, Tang RY. The optimization of pole arc coefficient to reduce cogging torque in surface-mounted permanent magnet motors. IEEE Transactions on Magnetics 2006; 42 (4): 1135-1138.

[2] El-Refaie AM. Fractional-slot concentrated-windings synchronous permanent magnet machines: Opportunities and challenges. IEEE Transactions on Industrial Electronics 2010; 57 (1): 107-121.

[3] Zhu ZQ, Wu LJ, Mohd Jamil ML. Distortion of back-EMF and torque of PM brushless machines due to Eccentricity. IEEE Transactions on Magnetics 2013; 49 (8): 4927-4936.

[4] Xu L, Zhang C, Zhu X, Lin M, Zheng S. Indirect analytical modeling and analysis of V-shaped interior PM synchronous machine. IEEE Access 2019; 7: 173786-173795.

[5] Zhu ZQ, Wu LJ, Xia ZP. An accurate subdomain model for magnetic field computation in slotted surface-mounted permanent-magnet machines. IEEE Transactions on Magnetics 2010; 46 (4): 1100-1115.

[6] Zhou Y, Li H, Meng G, Zhou S, Cao Q. Analytical calculation of magnetic field and cogging torque in surface-mounted permanent-magnet machines accounting for any eccentric rotor shape. IEEE Transactions on Industrial Electronics 2015; 62 (6): 3438-3447.

[7] Tabatabaei I, Faiz J, Lesani H, Razavi MTN. Modeling and simulation of a salient-pole synchronous generator with dynamic eccentricity using modified winding function theory. IEEE Transactions on Magnetics 2004; 40 (3): 1550-155.

[8] Mahmoud H, Bianchi N. Eccentricity in synchronous reluctance motors—part I: analytical and finite-element models. IEEE Transactions on Energy Conversion 2015; 30 (2): 745-753.

[9] Mahmoud H, Bianchi N. Eccentricity in synchronous reluctance motors—part II: different rotor geometry and stator windings. IEEE Transactions on Energy Conversion 2015; 30 (2): 754-760.

[10] Qian H, Guo H, Wu Z, Ding X. Analytical solution for cogging torque in surface-mounted permanent-magnet motors with magnet imperfections and rotor eccentricity. IEEE Transactions on Magnetics 2014; 50 (8): 1-15.

[11] Fu JJ, Zhu CS. Subdomain model for predicting magnetic field in slotted surface-mounted permanent-magnet machines with rotor eccentricity. IEEE Transactions on Magnetics 2012; 48 (5): 1906-1917.

[12] Rahideh A, Korakianitis T. Analytical open-circuit magnetic field distribution of slotless brushless permanent-magnet machines with rotor eccentricity. IEEE Transactions on Magnetics 2011; 47 (12): 4791-4808.

[13] Li Y, Lu Q, Zhu ZQ, Wu LJ, Li GJ et al . Analytical synthesis of air-gap field distribution in permanent magnet machines with rotor eccentricity by superposition method. IEEE Transactions on Magnetics 2015; 51 (11): 1-4.

[14] Alam FR, Abbaszadeh K. Magnetic field analysis in eccentric surface-mounted permanent-magnet motors using an improved conformal mapping method. IEEE Transactions on Energy Conversion 2016; 31 (1): 333-344.

[15] Jalali P, Boroujeni ST, Bianchi N. Simple and efficient model for slotless eccentric surface-mounted pm machines. IET Electric Power Applications 2017; 11 (4): 631-639.

[16] Boroujeni ST, Jalali P, Bianchi N. Analytical modeling of no-load eccentric slotted surface-mounted PM machines: cogging torque and radial force. IEEE Transactions on Magnetics 2017; 53 (12): 1-8.

[17] Boroujeni ST, Emami SP, Jalali P. Analytical modeling of eccentric PM-inset machines with a slotless armature. IEEE Transactions on Energy Conversion 2019; 34 (3): 1466-1474.

[18] Yu SB, Tang RY. Electromagnetic and mechanical characterizations of noise and vibration in permanent magnet synchronous machines. IEEE Transactions on Magnetics 2006; 42 (4): 1335-1338.

[19] Lin F, Zuo S, Deng W, Wu S. Modeling and analysis of electromagnetic force, vibration, and noise in permanent-magnet synchronous motor considering current harmonics. IEEE Transactions on Industrial Electronics 2016; 63 (12): 7455-7466.

[20] Torregrossa D, Khoobroo A, Fahimi B. Prediction of acoustic noise and torque pulsation in PM synchronous machines with static eccentricity and partial demagnetization using field reconstruction method. IEEE Transactions on Industrial Electronics 2012; 59 (2): 934-944.

[21] Han H, and Liu JL. Study of rotor eccentricity effect on permanent magnet servo motor performance. Electric Machines and Control 2016; 20 (1): 52-59 (in Chinese with an abstract in English).

[22] Li QF, Huang SR, Huang HJ. Noise and torque characteristics of permanent magnet synchronous motor with unequal pole arc structure. Journal of Zhejiang University(Engineering Science) 2018; 52 (11): 173-180 (in Chinese with an abstractin English).

[23] Boroujeni ST, Mohammadi AA, Oraee A, Oraee H. Approach for analytical modelling of axial-flux PM machines. IET Electric Power Applications 2016; 10 (6): 441-450.

[24] Wang XH, Li QF, Wang SH, Li QF. Analytical calculation of air-gap magnetic field distribution and instantaneous characteristics of brushless DC motors. IEEE Transactions on Energy Conversion 2003; 18 (3): 424-432.

[25] Wang X, Sun X, Gao P. Study on the effects of rotor-step skewing on the vibration and noise of a PMSM for electric vehicles. IET Electric Power Applications 2020; 14 (1): 131-138.